THE JOURNAL OF PHYSICAL CHEMISTRY B

ARTICLE

pubs.acs.org/JPCB

Intraligand Hydrophobic Interactions Rationalize Drug Affinities for Peptidyl−Prolyl Cis−Trans Isomerase Protein

Marco Bizzarri,[†] Simone Marsili,[†] and Piero Procacci*[,†,‡]

[†]Dipartimento di Chimica, Università di Firenze, Via della Lastruccia 3, I-50019 Sesto Fiorentino, Italy

[‡]Centro Interdipartimentale per lo Studio delle Dinamiche Complesse (CSDC), Via Sansone 1, I-50019 Sesto Fiorentino, Italy

Supporting Information

ABSTRACT: The conformational landscape of three FK506-related drugs with disparate inhibition constants is determined in bulk solution using a replica exchange simulation method with solute torsional tempering. Energetic fitness of important drug conformations with respect to the FKBP12 protein is evaluated by molecular mechanics. Results show that the experimental affinity toward peptidyl−prolyl cis−trans isomerase protein (FKBP12) of the analyzed ligands appears to be positively correlated to the observed population of specific chair structures of the drug piperidinic ring in bulk solution. This observation is rationalized on the basis that such structures, stabilized by stereospecific intramolecular hydrophobic interactions, allows the formation of a pair of protein−ligand hydrogen bonds upon binding.

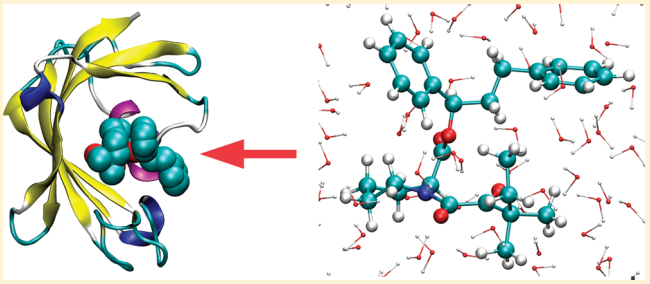

1. INTRODUCTION

The macrolide tacrolimus drug (also known as FK506) and its derivatives have attracted great attention in the last years due to the immunosuppressant properties when bound to the cytosolic FKBP12 protein.[1] The resulting complex serves as an inhibitory ligand to calcineurin, a cellular target for signal transduction in antigen specific T-cells activation and proliferation[2−4] and, for this function, termed as the "Achilles' heel" of the immune system.[5] Because of their immunosuppressant power, FK506-related drugs are since years routinely used after allogeneic organ transplant to reduce the activity of the patient's immune system and so lower the risk of organ rejection. Also, recent evidence[6,7] of the efficacy of FK506 and rapamycin have been produced in animal models of human multiple sclerosis. In particular, oral or intraperitoneal treatment with rapamycin, at the peak of disease or at the end of the first clinical attack, dramatically ameliorated the clinical course of experimental autoimmune encephalomyelitis in mice.[7]

Concerning specifically FKBP12 inhibition, the FK506−FKBP12 complex has been found to interfere in the interaction of FKBP12 with amyloidogenetic proteins.[8] FK506 binding protein FKBP12 has in fact been shown to be expressed at higher level in areas of pathologies of patients affected by neurodegenerative disease,[8] possibly due to its peptide prolyl isomerase activity.[9] With this respect, FKBP12 is believed to have a role in amyloid fibrils aggregation in Alzheimer and Parkinson diseases, promoting cis−trans isomerization of proline,[8,9] often the rate-limiting event in protein folding.

The naturally produced drug FK506[10] as well as its known analogues, including rapamycin,[11] bind the FKBP12 protein through two hydrogen bonds between the donors OH of Tyr82 and NH of Ile56 and the acceptors carbonyl groups (C8−O3 and C1−O2) in the pipecolyl α-keto amide region. Because of its dual role as immunosuppressant (in complex with FK506) and as rotamase activator, in the recent past FKBP12 has been the target of various studies aimed at discovering and designing drugs that can form immunosuppressant active complexes or that may inhibit its binding properties with respect to other proteins.[1,12−17] Most of the experimental works, in a typical QSAR spirit, focused in the synthesis and characterization of families of compounds having a common pipecolyl α-keto amides core, i.e., the buried moiety of FK506 or rapamycin when bound to the FKBP12 protein to form the immunosuppressant complex.[12,18] From a theoretical standpoint, much attention has been devoted in the evaluation of the binding free energy for FK506 parent compounds adopting various methodologies such as free energy perturbation,[19,20] linear response method,[21] continuum solvent and Poisson−Boltzmann approaches,[22] and the QM/MM method.[23]

In the present study we examine, from a computational standpoint, the effect of the piperidinic ring boat-chair equilibrium in water solution on the conformational properties of some FKBP12 ligands, all based on common pipecolyl α-keto amides moiety, with disparate experimentally known inhibition constants,[12,18] with the aim of detecting possible correlations between the conformational properties of the ligands and their

Received: November 5, 2010
Revised: January 24, 2011
Published: April 18, 2011

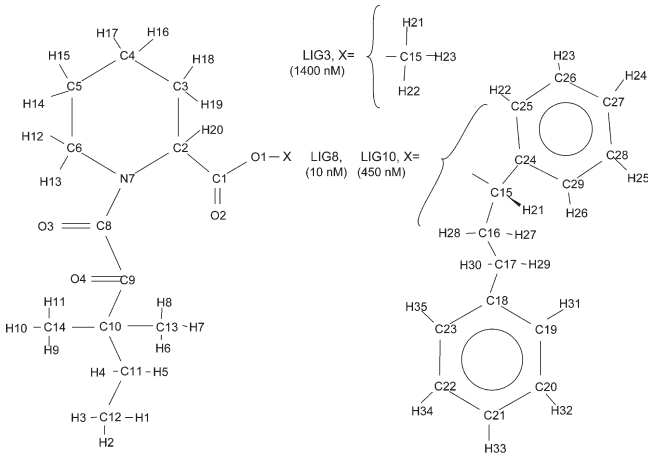

Figure 1. Chemical structure of the ligands. In parentheses we also report the FKBP12 inhibition constants.[18]

FKBP12 inhibitory power. To this end, we have parametrized the force field for LIG3, and the two stereoisomers LIG8 and LIG10 (see Figure 1). For each ligand, we have performed constant temperature-constant pressure molecular dynamics simulations in explicit water using a solute tempering Hamiltonian replica exchange method (REM).[24−27] In particular, within the solute (i.e., the ligands), exploiting the high grade of cooperativity in torsional transitions in these molecules, only the torsional and 14 nonbonded potentials were scaled along the replica progression, with an important reduction of the number of needed replicas for an effective sampling of the conformational space of the ligand. Bidimensional free energy maps as a function of the piperidinic ring dihedrals were obtained for each ligand in solution, showing and quantifying the prevalence of specific chairlike conformations over boat or twisted boat configurations at standard conditions for temperature and pressure. Within chairs conformation, we found that the most populated clusters are characterized by O2−O3 distances in the range 4−5 Å, i.e., the distance between these two carbonyl oxygen atoms in the experimentally determined structures of the FKBP12 complexes.[11,12] By using molecular mechanics calculations, for each ligand we evaluated the energetic fitness[28] of the most and least populated conformations found in solution with the FKBP12, showing that the conformations that best fit in the FKBP12 pocket are precisely those that exhibit an O3−O2 distance of 4−5 Å, allowing the formation of the hydrogen bonds O3-Tyr82 and O2-Ile56. Remarkably, the experimental inhibition constants of the analyzed ligands appears to be positively correlated to the observed population, in bulk solution, of chair structures with the piperidine C2 substituent in axial position. Such structures, stabilized by stereospecific intraligand hydrophobic interactions, exhibit mean O2−O3 distances in the range 4.2−4.6 Å and, hence, the best energetic fitness with respect to the FKBP12 protein making them fit for FKBP12 binding. The results presented in this study constitute, in our view, a rationalization of the effectiveness of FK506 derived drugs with respect to FKBP12 inhibition providing a valuable clue for designing new and more effective compounds.

The paper is organized as follows: in section 2 we discuss and present the AMBER[29] based force field derived for LIG3, LIG8 and LIG10. In the same section the theoretical and computational details of the solute tempering Hamiltonian REM molecular dynamics simulations are described. In section 3, the results of the REM simulations for LIG3, LIG8 and LIG10 are presented with emphasis on the conformational distribution of the piperidinic ring and the impact on in its FKBP12 binding affinity. In the same section, extensive molecular mechanics calculations, aimed at assessing the energetic fitness of the ligands when bound to FKBP12, are presented. In section 4, results are discussed and a rationalization of the inhibitory power of the ligands is proposed. Conclusive remarks and perspective are discussed in section 5.

2. METHODS

Force Field for the Ligands. The chemical structure of the FK506-derived ligands LIG3, LIG8 are reported in Figure 1 with atomic name assignment taken directly from the PDB file with id code 1FKG.[12] LIG10 is the stereoisomer of LIG8 obtained from the latter by reflection with respect to the C15−H21−O1 plane. The force field for these ligands in solution is based on the AMBER03 parametrization.[30] The atomic type assignment of all atoms in LIG3, LIG8, and LIG10 is reported in Table 1 of the Supporting Information. The atomic charges (reported in Table 1 of the Supporting Information) have been calculated using the following methodology. The initial geometry of LIG8 was taken from the crystal structure of the FKBP12 complex.[12] Hydrogen atoms were added using the ORAC program.[31] LIG3 was also generated from the crystal structure of LIG8 in the complex by severing the phenyl and the ethyl-benzene moieties from carbon C15 and by adding the two saturating hydrogen to C15 using again the ORAC suite.[31] The initial structure of the stereoisomer LIG10 was generated from that of LIG8 by mirror reflection with respect to the plane C15−C24−O1 involving the asymmetric carbon C15. These initial structures of LIG3, LIG8, and LIG10 underwent a geometry optimization using density functional theory (DFT) with the B3LYP exchange-correlation functional[32] and using the split valence 631-Gd basis set. On the optimized geometries of LIG3 and LIG8, we calculate, at the same level of theory, the atomic charges using the electrostatic potential fit (ESP) according to the Merz−Singh−Kollman scheme.[33] Equivalent charges (e.g., charges on the hydrogen atoms of methyl groups) have been symmetrized. The atomic charges of LIG8 are transferred with no modification to its stereoisomer LIG10. Given the flexibility of the solubilized ligands at room temperature, in order to assess the dependence of the ESP charges on the local minimum geometry, we performed *ab initio* calculation on two significantly different geometries of LIG3 obtained by geometry optimization at the DFT-B3LYP/631Gd level of starting structures sampled from high temperature MD simulations *in vacuo* using the force field defined in Table 1 of the Supporting Information. Results shows that the ESP charges for this LIG3 depends in a negligible way on the geometrical conformation of the local minimum. Similarly, we found that the ESP charges on the common part of LIG3 and LIG8/10 do not differ significantly (see Figure 1 in the Supporting Information).

Molecular Dynamics Simulation. The REM simulation for each ligand was performed using the Hamiltonian REM approach as enforced in the program ORAC.[27] Only the torsional potential of the ligand was scaled throughout the replica progression with a maximum and minimum scaling factors (1.0, 0.3) corresponding to a "temperature" of 300 K and of 900 K, respectively. The potential energy for the *k*th replica is then

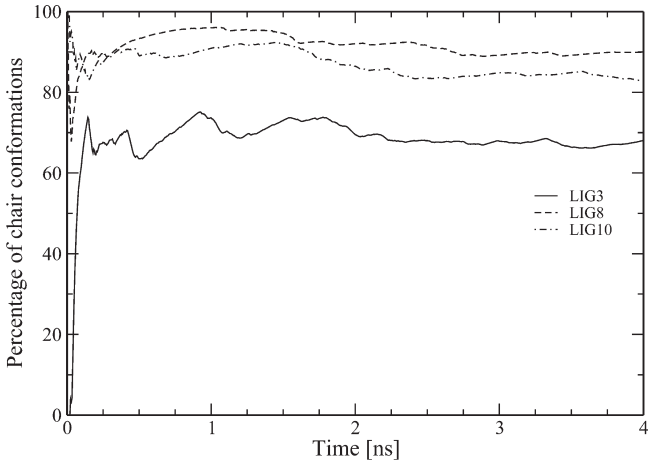

Figure 2. Running average of the percent fraction of chair conformations in the target replica (torsional scaling factor 1.0) for the 4 ns REM/torsional tempering simulation.

given by $V_k = V + (c_k - 1)V_T^{[ligand]}$ where V is the full potential energy of the system, $V_T^{[ligand]}$ is the torsional potential (including 1−4 nonbonded interactions) of the ligand alone, and c_k is the torsional scaling factor. Such a solute tempering approach,[34] by reducing the degrees of freedom that are involved in the scaling in the generalized ensemble (i.e., only those affected by the proper and improper torsions of the ligand), allows one to minimize, for a given replica exchange rate, the number of replicas needed in the given scaling range (300−900 K) while maintaining at same time a high flexibility of the ligand in the "hot" replicas. Using such an approach a very efficient exploration of the solute conformational space can be obtained at a very limited computational cost. Since most of the degrees of freedom (including those of explicit water) are not involved in the scaling and since the operating effective temperature is 300 K for all replicas, the sample remains in the liquid state at all torsional temperatures. In these thermodynamics conditions, the Hamiltonian REM simulation can be performed in the isothermal−isobaric ensemble thus allowing the molar volume to readjust in a transition between the solute conformational states at standard external pressure.

At step zero, the ligand in the *ab initio* optimized geometry was placed for at the center of a cubic simulation box with side length of 25 Å along with 512 TIP3[35] water molecules disposed on a regular simple cubic lattice. Water molecules yielding bad contacts with the ligand atoms were discarded, thus obtaining 505 and 497 molecules for LIG3 and LIG8/LIG10, respectively. Constant temperature (300 K) was enforced using a Nosé−Hoover thermostat[36] while the external pressure of 0.1 MPa was imposed using a modification of the Parrinello−Rahman Lagrangian allowing for isotropic volume changes.[37] The electrostatic interaction were treated using the smooth particle mesh Ewald method,[38] with 16 grid points in each directions and a 4th order B-spline interpolation. The equations of motion were integrated using a multiple time step r-RESPA algorithm[39] with a potential subdivision specifically tuned for biomolecular systems.[31,37] In the first 100 ps of the simulation, no exchanges between the eight replicas were attempted. This preliminary step served for solvent and volume equilibration, yielding a replica independent mean side length of the cubic box of 25.21(1) Å for LIG3, 25.19(1) Å for LIG8, and 25.20(1) for LIG10. As previously stated, the replicas differ only in the torsional potential whose scaling factors, c_k, were chosen such that the corresponding effective torsional temperature of the eight replicas is distributed in the given range with a temperature progression according to scheme given in ref 26. In the production stage, exchanges between adjacent replicas were attempted every 100 fs and conformations were saved every 0.5 ps producing a total of 8000 configurations per replica. The REM simulation for each ligand totalizes 32 ns (4 ns per replica). In spite of the wide torsional temperature range, due to the limited amount of degrees of freedom involved in the Hamiltonian scaling, eight replicas were sufficient, for all ligands, to obtain exchange acceptance ratios in the range 0.5−0.75. In Figure 2, we report the running average of the fraction of the chair conformation for the piperidinic ring of the bulk solution of LIG3, LIG8 and LIG10 for the target replica (torsional scaling factor 1.0). It can be seen that, approximately after 2 ns, the fraction of chair conformations reaches a stationary value no matter what the starting configuration of the solute was. In particular, LIG3, starting from an optimized boat conformation, quickly evolves into a state with a majority of chair structures. Error bars on the conformational distributions are rather small and have been evaluated by repeating two independent additional 32 ns REM simulations on LIG8. Results of the error analysis are reported in Table 1.

Table 1. Estimated Percent Probabilities for Piperidinic Ring Conformations and Their Respective Mean O2−O3 Distances (R_{oo}/Å)[a]

	LIG3		LIG8		LIG10	
ring conformation	LIG3	R_{oo}	%	R_{oo}	%	R_{oo}
6C1	11.8	4.33	18.20 ± 1.71	4.71 ± 0.09	15.6	4.45
6C2	1.4	3.18	0.23 ± 0.06	3.35 ± 0.12	0.3	3.20
6C3	31.3	4.10	36.60 ± 1.24	4.39 ± 0.11	34.4	4.14
6C4	0.9	3.24	0.17 ± 0.06	3.29 ± 0.10	0.2	3.12
6C5	21.1	4.06	30.33 ± 2.89	4.45 ± 0.12	32.3	4.18
6C6	1.6	3.23	0.33 ± 0.06	3.48 ± 0.05	0.3	3.25
6B1	0.4	3.62	0.10 ± 0.00	3.88 ± 0.20	0.1	3.69
6TB1	0.8	3.68	0.53 ± 0.38	3.89 ± 0.22	0.2	4.04
6B2	0.3	3.18	0.00 ± 0.00	-	0.1	3.31
6TB2	0.0	-	0.00 ± 0.00	-	0.0	-
6B3	4.5	3.69	2.47 ± 1.43	3.99 ± 0.35	1.9	3.90
6TB3	14.6	3.69	5.17 ± 0.87	4.14 ± 0.33	9.3	3.98
6B4	0.0	-	0.00 ± 0.00	-	0.0	-
6TB4	0.0	-	0.00 ± 0.00	-	0.0	-
6B5	3.3	3.75	1.50 ± 0.66	4.22 ± 0.17	2.9	3.97
6TB5	0.3	4.03	0.13 ± 0.06	3.99 ± 0.28	0.1	4.10
6B6	4.3	3.50	3.20 ± 1.65	3.76 ± 0.21	1.4	3.60
6TB6	3.0	3.29	0.77 ± 0.12	3.52 ± 0.13	0.8	3.37

[a] Data for LIG8 have been calculated by averaging the conformational probabilities obtained from three independent REM simulations in series of equal length (4 ns).

3. RESULTS

Potential of Mean Force of LIG8 in Bulk Solution. For LIG8, using the 8000 configurations sampled in the 4 ns simulation of the target replica, we calculated the potential of mean force along

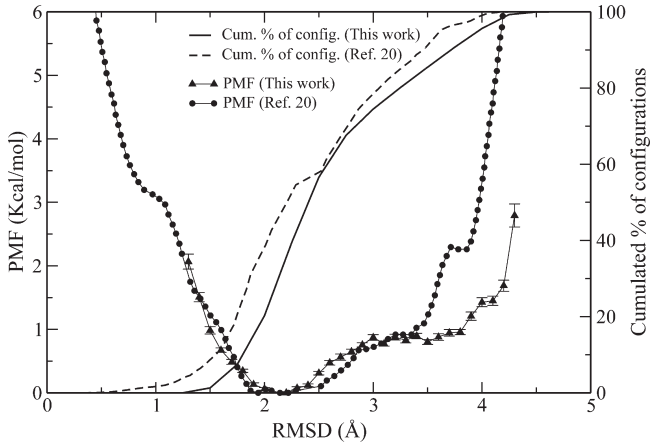

Figure 3. Potential of mean force and cumulative probability as a function of the rmsd from the configuration of LIG8 in the LIG8−FKBP12 complex.[12] Error bars for the PMF were estimated using Monte Carlo bootstrap analysis.

the root-mean-square displacement (rmsd) with respect to the experimental X-ray conformation of LIG8 in complex with FKBP12.[12] The rmsd coordinate is a rather unspecific one, as many unrelated structures can be compatible with a given value of the rmsd especially for large values of the coordinate. However, such a PMF was already measured in a past study on the FKBP12 binding free energies of FK506 derived compounds by Wang et al.[20] using an umbrella sampling approach with 21 sampling windows equally distributed in the rmsd coordinate range 0−5 Å and unbiasing the results with the weighted histogram analysis method.[40] In their paper, the force field for LIG8 was based on an unpublished AMBER03 parametrization (provided by M. R. Shirts as personal communication) with atomic charges calculated using the semiempirical approach AM1/BCC.[41] Comparison between our PMF (ligand force field based on AMBER03 with B3LYP/631Gd atomic charges and Hamiltonian REM/torsional tempering) and the PMF of Wang et al.[20] (AMBER03 parametrization with PM1/BCC atomic charges and multiple windows umbrella sampling) can thus provide a stringent double validation test for both the reliability of the force field for the ligand proposed in this study (Table 1 of the Supporting Information) and for the effectiveness of the undriven torsional tempering technique in the conformational sampling of flexible molecules with high torsional barriers.

In Figure 3 we report the PMF and the corresponding underlying cumulative probability calculated in our simulation and in that of Wang et al.. The agreement is in general satisfactory, especially in the range 1.25−3.5 Å where most of the conformations occur. More in detail, both PMF's exhibit a stretched minimum at about 2−2.5 Å with the PMF calculated using the torsional tempering approach growing less rapidly than that of Wang for rmsd ≥ 3.5 Å, thus implying that configurations that are more than 4.0 Å away in rmsd metric from the crystal structure have a non negligible probability to occur. Given the flexibility in solution and the size of the ligand and given the high unspecificity of the rmsd coordinate for large values (i.e., more and more structures are compatible with large values of the rmsd distance form the crystal structure), our result appears definitely more reasonable than that obtained with the Umbrella sampling approach whereby configurations with *rmsd* ≥ 4.2 are very unlikely to be observed, thus confirming the effectiveness of the torsional tempering approach in sampling the conformational space of flexible molecules. Such a result is important as, for ligands in bulk solution, the torsional tempering approach has the same computational cost of the umbrella sampling method (few tens of nanoseconds in total) but the former, being a coordinate-free method, may be used, unlike the latter, to calculate in the postanalysis phase free energy surfaces along arbitrarily selected system coordinates.

Conformational Analysis in Bulk Solution. As stated in the introduction, FK506-related ligands bind the FKBP12 protein through two hydrogen bonds between the protein donors OH of Tyr82 and the backbone NH of Ile52 and the acceptors carbonyl groups (O3 and O2 in Figure 1) in the pipecolyl α-keto amide region. Optimal ligand binding in experimentally known ligand−FKBP12 complexes[11,12] seemingly occurs when the distance between O2 and O3 is between 4 and 5 Å. The O2−O3 distance in the ligand depends on the dihedral C1−N7−C2−C8 whose value is in turn affected by the dihedrals of the piperidinic ring. In the light of such considerations, using the 8000 configurations of the target replica, we analyzed the conformational structure assumed by the piperidinic ring of the ligands in bulk solution to quantify the correlation between the mean O2−O3 distance and the piperidinic ring conformation and the corresponding FKBP12 inhibition constant. The various ring conformations have been classified according to the convention proposed by Espinosa.[42,43] Such a convention is based on the symmetry elements of the ring and on the signs of the intracyclic dihedral angles. In the Supporting Information (Figure 2), we report the classification scheme for the chair (C) conformations and for the boat/twisted boat (B, TB) conformations. The results of the conformational analysis are reported in Table 1. Inspection of the table indicates that the more likely four conformations of the piperidinic ring in bulk solution are the same for all three ligands and that the chair conformations are by far more abundant than the boat or twisted boat conformations. In particular, according to our torsional tempering simulations, the 6C3, 6C5, 6C1 types (see Supporting Information for the definition) are the likeliest piperidinic ring conformation in bulk solution and are all characterized by the axial orientation of the C2 ring substituent. Comparing the conformational distributions of the three ligands, we note that the overall likelihood of chair conformations increases in the series LIG3 (64.2%), LIG10 (82.3%) LIG8 (85.1%), reflecting the increase of the corresponding FKBP12 affinity[12,18] (K_i = 1600 nM for LIG3, K_i = 450 nM for LIG10, and K_i = 10 nM for LIG8). This fact indicates that the mean piperidinic ring conformation of the ligand in bulk could an important ingredient in determining its affinity to the FKBP12 protein and that an increase of the likelihood of chair conformation in bulk solution possibly enhances the inhibitory power of the ligand. This correlation between binding affinity and incidence of chair conformation in bulk can be rationalized with the aid of Table 1 where we also report the mean O2−O3 distance for solute configurations belonging to the various piperidinic ring conformations. It can be seen that the more likely chair conformations (i.e., 6C1, 6C3 and 6C5) are characterized by mean O2−O3 distances in the range 4−5 Å. Such ligand conformations are suitable to bind the FKBP12 protein. As a matter of fact, in the FKBP12 complex with the FK506 related ligands LIG8 and Rapamycin, both ligands binds the FKBP12 protein with two hydrogen bonds involving Tyr86 and Ile56 and are found in the axial chair conformation C3 with O2−O3 distance equal to 4.6 Å.[11,12,18] Further details on the energetics of the conformational

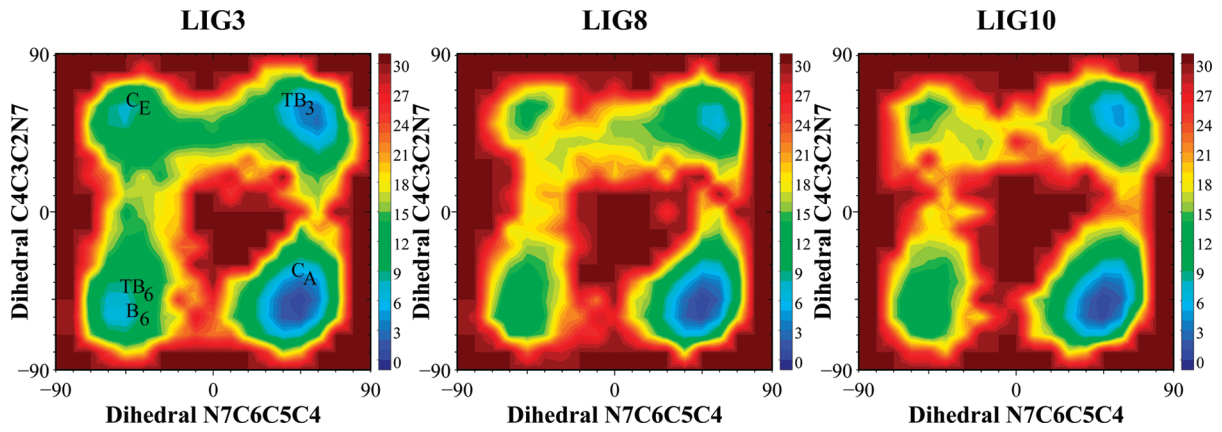

Figure 4. Piperidinic ring conformational free energy maps [kJ mol^{-1}] with respect to the dihedral coordinates: C4C3C2N7 and N7C6C5C4 (see Figure 1 for atom name definitions).

space of the three ligands can be achieved by calculating free energy surfaces with respect to specific collective coordinates. In particular, for each ligand, the 2D distribution function $P(\theta_1,\theta_2)$ with respect to opposite piperidinic ring dihedral angles and the associated free energy $G = -RT \ln P(\theta_1,\theta_2)$ was calculated using all of the 64000 configurations from the torsional REM simulation by applying the multiple Bennett acceptance ratio.[44] Using such method, the statistics at high torsional temperatures is used, with an appropriate weight, to reconstruct the peaks the free energy barriers that are normally not sampled at the target (unscaled) replica.

In Figure 4, we collect the free energy surfaces obtained for LIG3, LIG8, and LIG10 as a function of the two opposite dihedral angles N7C6C5C4 and C4C3C2N7. These maps feature a similar pattern for all ligands with four different minima located in different quadrants. As one can see from Figure 2 of the Supporting Information, the chair conformations are characterized by opposite dihedrals with opposite signs (upper left and lower right quadrants). Hence, axial and equatorial chair conformations of the C2 piperidinic ring substituent (C_A, C_E) have positive and negative N7C6C5C4 and C4C3C2N7 dihedral angles, respectively. So the deepest minimum in the lower right quadrant corresponds to the C_A configuration while the high energy state in the upper left quadrant refers to the C_E structure. Twisted boat conformations have nonzero N7C6C5C4 and C4C3C2N7 dihedral angles of equal sign. Positive dihedrals (upper right quadrant) include the important secondary minimum 6TB3 while negative dihedrals characterize the less likely intermediates 6TB6 and 6TB1. The boat structures with a pair of approximately zero opposite dihedral angles are basically unstable and no minimum corresponding to these structure shows up in the free energy map with respect to the N7C6C5C4 and C4C3C2N7 dihedral angles and with respect to other opposite dihedral pairs (data not shown). The equatorial-axial position exchange for chair conformations occurs through a twisted boat intermediate whose stability grows in the series LIG8, LIG10, and LIG3. Conversely, the stability of the chair axial structure increases in the series LIG3, LIG10, and LIG8. The minimum free energy path for the $C_A \leftrightarrow C_E$ interconversion occurs in all ligand through the surmounting of two free energy barriers in series whose height (4−5 kcal mol^{-1}) is larger for LIG8 and LIG10. The mutual orientation of the two carbonyl units, C1−O2 and C8−O3, which is crucial for FKBP12 binding, is related to the mutual arrangement of the dihedral involving the C2 and N7 substituents, i.e., O3C8N7C2 and O2C1C2N7, respectively. When the former is in cis and the latter in trans configuration, the orientation of the carbonyl and the O2−O3 distance (around 4.5 Å) is optimal for binding (see also Figure 3 of the Supporting Information). This outcoming can occur with a significant probability only when the C2 piperidinic ring substituent is in axial(perpendicular) configuration. In LIG8, and to a much lesser extent in the stereoisomer LIG10, this optimal cis−trans arrangement of the O3C8N7C2 and O2C1C2N7 dihedrals (with the C2 substituent in axial position) is favored by hydrophobic interactions. In particular, in LIG8 we register a strong and stereospecific interaction (that is not observed in the less potent LIG10) of the (1,1)dimethyl propyl group of the N2 substituent with one phenyl ring of the C2 substituent. In Figure 5 we report the probability contact maps between hydrophobic carbon atoms for LIG8 and LIG10. Atom−atom contacts have been counted according to function[45] $C_{ij} = 1$ if $r_{ij} < \delta$ and $C_{ij} = [1 - (r_{ij} - \delta)^6]/[1 - (r_{ij} - \delta)^{12}]$ if $r_{ij} \geq \delta$ where r_{ij} is the atom atom distance and δ = 5 Å. The probability for an ij carbon−carbon contact is thus defined as $P_{ij} = N^{-1}\Sigma_k^N C_{ij}^{(k)}$, where the sum goes over the N 8000 configurations and $C_{ij}^{(k)}$ is the contact function of the ij hydrophobic carbon pair in the kth configuration.

From Figure 5, we see that in LIG8 there is a likely contact between the (1,1)dimethyl propyl group and the phenyl group C24−C29 and a less likely contact between the piperidinic ring and the ethyl-phenyl group due mostly to pseudostacked arrangements. In the stereoisomer LIG10 such contacts are not present and a much weaker contact involves the (1,1)dimethyl propyl group and the ethyl-phenyl group (aromatic group 1, C16−C23). The correlation between the hydrophobic group spatial arrangement in LIG8/LIG10 and the conformation of the carbonyl units is further detailed in Figure 4 of the Supporting Information.

From Figure 6, we can finally quantify, for the three ligands, the overall impact of these hydrophobic interactions on the probability distributions of the rmsd from the experimental crystal structure[12] calculated for the atoms involving the two binding carbonyl units (C8−O3 and C1−O2). The amount of bulk configurations with the carbonyl units in crystal-like configurations grows in the series LIG3, LIG10, and LIG8. In LIG3, due to the absence of the aromatic groups, carbonyl crystal-like

dx.doi.org/10.1021/jp110585p |J. Phys. Chem. B 2011, 115, 6193–6201

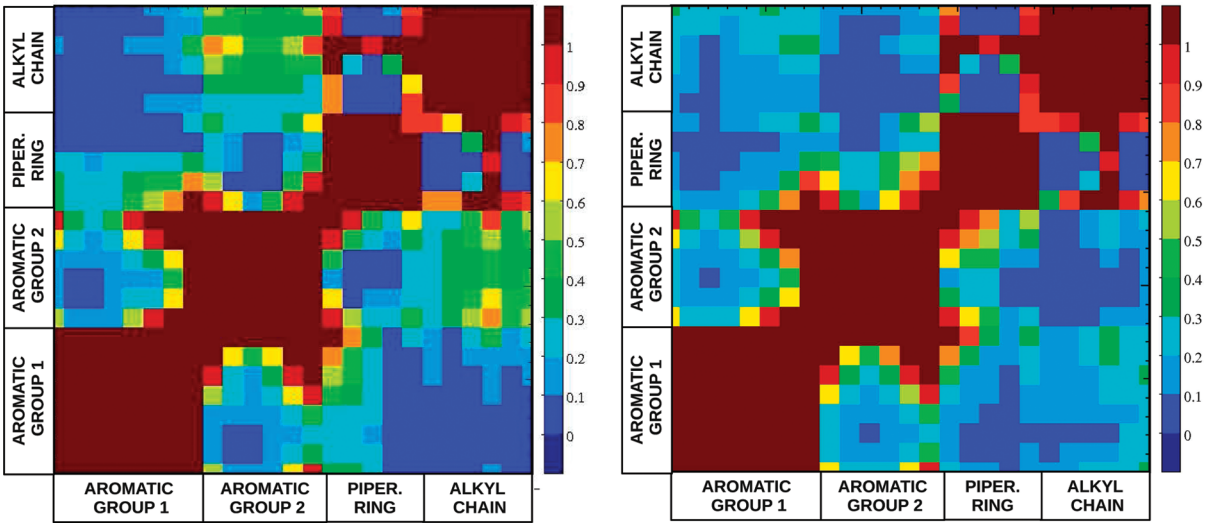

Figure 5. Probability contact map P_{ij} (see text for definition) for the hydrophobic carbons in the two stereoisomers LIG8 (left) and LIG10 (right). The aromatic group 1 includes carbons C16−C23. The aromatic group 2 includes carbons C24−C29. The piperidinic group includes carbons C2−C6. The alkyl chain group include the carbons (C10−C14) of the (1,1)dimethyl propyl group.

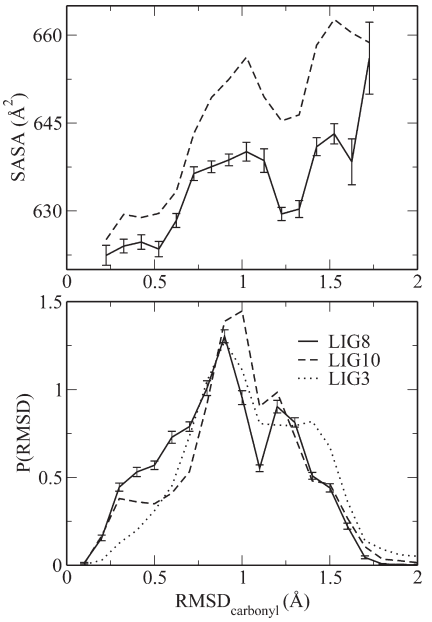

Figure 6. Bottom panel: Distributions of rmsd for the carbonyl units of LIG3, LIG8, and LIG10 from the experimental structure[12] of the ligand-protein complex of LIG8. Structures were aligned on the ring atoms (C2, C3, C4, C5, C6, N7) and rmsd were computed on the carbonyl atoms (C1, O2, C8, O3). Top panel: Average solvent accessible surface area (SASA) of carbon atoms for LIG8 and LIG10 as a function of the carbonyl rmsd. SASA calculations were performed using 1.4 Å as the probe radius. Error bars were estimated using Monte Carlo bootstrap analysis.

conformations (rmsd <0.5 Å) are not stabilized. In LIG8 the stabilization of crystal like structures of the carbonyl units is approximately twice as much as in LIG10. The hydrophobic stabilization of the crystal-like ligand configuration is clearly supported by the trend of the average solvent accessible surface area (SASA) of ligand carbon atoms as a function of the carbonyl rmsd, as shown in the top panel of Figure 6 for LIG8 and LIG10. SASA was computed using the GEPOL93 code.[46] Ligand structures with carbonyl units close to the experimental bonding configuration clearly correspond to the global minimum of the solvent exposed hydrophobic surface.

Ligand−FKBP12 Energetic Fitness. The binding free energy of a ligand is the result of several competitive contributions, including positive ones such as translational, rotational and conformational entropy loss upon binding and desolvation effects.[47] For a ligand to bind effectively, entropy and desolvation costs must be compensated by the negative contribution due to favorable interactions with the protein. In this section, we focus on this latter fundamental term by using a methodology outlined in ref 28 when evaluating the energetic fitness of histidine tautomers in proteins. Such analysis is aimed at determining the role of the energetic fitness at the binding site for the three ligands with disparate inhibition constants. The energetic fitness of the ligands was determined as follows. The starting configuration of the LIG8−FKBP12 complex was taken directly from the experimental structure of the PDB file with code 1FKG,[12] while for LIG3 and LIG10 we implemented the appropriate fragment substitutions and reflection by taking as template the structure of LIG8 in the complex LIG8−FKBP12. The conformational space of the binding site (i.e., only the ligand and its nearby residues are allowed to move while distal protein residues are maintained at their experimental position) was sampled in a series of 1 ns simulation in vacuo at T = 800 K. During these runs, the piperidinic ring can freely rotate and translate but is constrained to assume the chair (6C3) conformation corresponding to experimental structure, by imposing a series of intraring bond and angle restraints. The size of the sampled binding site varied in the three simulation, by freezing all protein atoms whose distance from any atom of the ligand exceeded 5, 6, and 7 Å (in the following such threshold distance defines the mobility radius R_M). In a inherent structure-like[48] approach, during each of the simulations we periodically quenched by steepest descent with respect to the binding site coordinates uncorrelated high temperature configurations, selecting, among all quenched structures, the three most energetically favorable local minima. Finally, for each of the nine minima (three for each

Table 2. Best Energy Ligand−FKBP12 Quenched Structures[a]

ligand	R_M	R_{oo}	R_{o3-HY}	R_{o2-HI}	U_F	u_F
Lig8	5	4.10	1.73	1.89	−63	−0.93
Lig8	5	4.30	1.71	1.84	−60	−0.89
Lig8	5	3.97	1.72	1.86	−61	−0.90
Lig8	6	4.10	1.71	1.85	−69	−1.02
Lig8	6	4.16	1.71	1.86	−64	−0.94
Lig8	6	4.46	1.75	1.93	−62	−0.91
Lig8	7	4.52	3.93	1.92	−59	−0.87
Lig8	7	4.49	1.77	1.95	−63	−0.93
Lig8	7	4.40	1.76	1.87	−61	−0.90
Lig10	5	4.30	1.78	2.07	−62	−0.91
Lig10	5	3.96	1.71	1.91	−64	−0.94
Lig10	5	4.12	3.71	1.91	−61	−0.90
Lig10	6	4.14	3.73	1.89	−59	−0.87
Lig10	6	4.57	1.74	1.91	−63	−0.92
Lig10	6	4.00	1.68	1.92	−64	−0.94
Lig10	7	3.82	1.72	1.88	−62	−0.91
Lig10	7	3.77	1.70	1.90	−63	−0.93
Lig10	7	4.58	1.82	1.92	−62	−0.92
Lig3	5	4.22	1.78	1.91	−46	−1.09
Lig3	5	4.09	1.78	1.92	−50	−1.18
Lig3	5	4.33	1.73	1.98	−48	−1.14
Lig3	6	4.14	1.79	2.08	−52	−1.25
Lig3	6	3.86	1.74	1.91	−57	−1.35
Lig3	6	4.01	1.77	1.98	−47	−1.12
Lig3	7	4.50	1.77	1.88	−48	−1.14
Lig3	7	4.01	1.73	1.86	−48	−1.14
Lig3	7	3.97	1.76	1.94	−55	−1.30

[a] Key: R_M, Mobility radius; R_{oo}, distance between atoms O2 and O3; R_{O3-HY}, distance between atoms O3 and HO of TYR82; R_{O2-HI}, distance between atoms O2 and HN of Ile56; U_F, energetic fitness; u_F, energetic fitness per ligand atom; all distances and energies are in Å and kcal mol^{-1}, respectively.

mobility radius R_M), the corresponding energetic fitness U_F was obtained by computing the difference between the minimized energy of the complex and that of the ligand and the FKBP12 protein in the same configuration at infinite distance.

Results are collected in Table 2. Inspection to the table shows that the U_F do not vary much for a given mobility radius and do not depend significantly on the ligand. In particular, the two stereoisomers LIG8 and LIG10 have very similar energetic fitness with that of LIG3 being slightly smaller. On the other hand, when considering the intensive quantity u_F, i.e the energetic fitness divided by the number of atoms of the ligand, LIG3 appears slightly more fit that LIG8 and LIG10 to bind FKBP12. Wang et al.[20] obtained for LIG8 an interaction free energy in the binding site of FKBP12 of −44 kcal mol^{-1}. Such value is expectedly smaller (from 5 to 10 kcal mol^{-1} with respect to ours, since it includes positive contributions such as, e.g., the entropic loss due conformational restraints of the ligand in the binding site with respect to bulk.

Going back to Table 2, it should be noticed that nearly all quenched structures are characterized by O2−O3 distances above 4 Å and bears the two H-bonds with FKBP12 involving OH(Tyr82)-O3 and NH(Ile56)-O2. This result indicate that the frozen piperidinic ring conformation allows the formation of these two specific H-bonds upon binding. When, during the quenching the piperidinic ring is kept in a configuration that is not likely to occur in bulk solution, such as the 6B1, the best quenched structures often do not exhibit optimal O2−O3 distance for H-bonding and correspondingly the energetic fitness Å is significantly diminished (data not shown).

In summary, when the piperidinic ring chair conformation allows the O2−O3 distance to be in the range 4−5 Å with no structural stress of the ligand, then the energetic fitness is essentially independent of ligand structure around pipecolyl α-keto amides core. Thus, it appears that the protein−ligand interaction, being comparable for all ligands, is not the driving force for explaining the observed differences in their inhibitory power.

4. DISCUSSION

The previous results can be summarized as follows. LIG8 has the largest affinity for the FKBP12 protein and has, in bulk solution, the C2 piperidinic ring substituent overwhelmingly in axial position. Such conformations produces, with important probability, structures where the O2−O3 distance is optimal for FKBP12 binding, stabilized by specific hydrophobic interactions. Because of the absence of the phenyl groups, this stabilization is not possible in LIG3 (which is in fact the weakest of the FKBP12 ligands) and is much less effective for the LIG8 stereoisomer LIG10. In the case of LIG8, these optimal configurations in bulk are very similar to those observed in the LIG−FKBP12 complex. On the other hand, the energetic fitness of the ligands (i.e., the mean protein ligand interaction energy *vacuo* obtained by quenching hot structures of Ligand in the FKBP12 active site) depends only on the distance O2−O3 and, in case the latter is optimal, is approximately the same for all ligands.

From the above analysis, we may thus conclude that the inhibitory power of the three analyzed ligand depends mostly on their capability of assuming the right O2−O3 configuration for binding in bulk solution, rather than on specific interactions between ligand substituents and protein residues. Therefore, the piperidinic ring conformation of the approaching ligand in bulk, though its influence on O2−O3 intraligand distance, plays a decisive role in its binding properties to FKBP12 by enabling (as in chair axial conformations) or not enabling (as in chair equatorial structures) the formation in the complex of the two H-bonds O3-HO(Tyr92) and O2-HN(Ile56).

As stated previously, the substituents of effective ligands such LIG8 are important not because they bind to specific residues in the active site of FKBP12, but since they stabilize through *intraligand* hydrophobic interactions the axial structures that favor the optimal O2−O3 distance for binding. Such considerations indeed suggest a possible route to design potent FK506-related drugs.

5. CONCLUSION AND PERSPECTIVES

In this paper we have studied, by means of atomistic molecular dynamics simulation, the conformational space in solution of three FK506-related ligands with disparate inhibition constant with respect to the FKBP12 protein. To this end we have derived an AMBER03 parametrization for simulating the ligands in explicit water. Given the large torsional barriers involved in the dynamics of the piperidinic ring (whose conformations influence the overall spacial arrangement of the ligand) in standard

conditions, the simulation have been performed using a solute tempering replica exchange approach with scaling of the ligand torsional potential, only.

The applied replica exchange methodology and the proposed force field have been validated, for LIG8, by comparing the PMF along the rmsd coordinate measuring the distance from the ligand in the crystal structure, to previous results in bulk obtained with earlier an parametrization and with the standard umbrella sampling technique.

The conformational analysis of the ligands in solution revealed the prevalence of chair structures with the C2 substituent of the piperidinic ring in axial position. Such structures exhibit in turn an important sub-ensemble of states with the O2−O3 distance around 4.5 Å.

Using a molecular mechanics approach we have shown that the conformations that best fit in the FKBP12 pocket (in terms of ligand protein interaction energy) are precisely those that exhibit an O3−O2 distance of 4−5 Å that allows the formation of the hydrogen bonds O3-Tyr82 and O2-Ile56. Remarkably, the FKBP12 inhibition constants of the ligands and the capability of the ligand to assume in bulk solution optimal O2−O3 distance for binding follows the series LIG3, LIG10, and LIG8. Hence, it appears that the effectiveness of FK506-related drugs for FKBP12 binding crucially depends on the piperidinic ring conformation of the approaching ligand *in bulk*, though its influence on the O2−O3 intraligand distance, by enabling, as in chair conformations with C2 substituent in axial position, the formation of the two H-bonds.

In the case of LIG8, the bulk substates with O3−O2 distance in the optimal range for FKBP12 binding are effectively stabilized by a 2-fold hydrophobic interaction where the 1,1-dimethyl propyl group of the N2 substituent interacts with the other phenyl ring of the C2 substituent and, to a lesser extent, one phenyl moiety of the C2 substituent insist on the piperidinic ring in pseudostacked arrangement. In LIG3, such hydrophobic stabilization is very weak due to the absence of the 1-(1,3-diphenyl)propyl moiety, while in LIG10, the overall spatial topology of the hydrophobic groups do not allows an interactions as effective as in its stereoisomer LIG8.

These results could provide, in our view, a valuable key for a rational drug design of FK506 related ligand.

■ ASSOCIATED CONTENT

Supporting Information. Complete references 3 and 17. Force field for FK506 related ligands, classification of the piperidinic ring conformations, and conformational properties in bulk. This material is available free of charge via the Internet at http://pubs.acs.org.

■ AUTHOR INFORMATION

Corresponding Author

*E-mail: procacci@unifi.it.

■ ACKNOWLEDGMENT

The present study has been funded by Regione Toscana.

■ REFERENCES

(1) Armistead, D. M.; Badia, M. C.; Deininger, D. D.; Duffy, J. P.; Saunders, J. O.; Tung, R. D.; Thomson, J. A.; Decenzo, M. T.; Futer, O.; Livingston, D. J.; Murcko, M. A.; Yamashitaand, M. M.; Navia, M. A. *Acta Crystallogr.* **1995**, *D51*, 522–528.

(2) Schreiber, M. K. R. M. S. L. *Angew. Chem., Int. Ed. Engl.* **1992**, *31*, 384–400.

(3) Kissinger, C. R.; et al. *Nature* **1995**, *378*, 641–644.

(4) Sieber, M.; Baumgrass, R. *Cell Commun. Signal* **2009**, *7*, 25–44.

(5) Crabtree, G. R.; Olson, E. N. *Cell* **2002**, 109.

(6) Gold, B. G.; Voda, J.; Yu, X.; McKeon, G.; Bourdette, D. *J. Neurosci. Res.* **2004**, *77*, 367–377.

(7) Esposito, M.; Ruffini, F.; Bellone, M.; Gagliani, N.; Battaglia, M.; Martino, G.; Furlan, R. *J. Neuroimmun.* **2010**, *220*, 52–63.

(8) Liu, F.; Liu, P.; Shao, H.; Kung, F. *Biochem. Biophys. Res. Commun.* **2006**, *350*, 472–477.

(9) Gerard, M.; Debyser, Z.; Desender, L.; Kahle, P. J.; Baert, J.; Baekelandt, V.; Engelborghs, Y. *FASEB J* **2006**, *20*, 524–526.

(10) Mo, S. J.; Ban, Y. H.; Park, J. W.; Yoo, Y. J.; Yoon, Y. J. *J. Ind. Microbiol. Biotechnol.* **2009**, *36*, 1473–1482.

(11) Van-Duyne, G.; Standaert, R. F.; Schreiber, S. L.; Clardy, J. *J. Am. Che. Soc.* **1991**, *113*, 7433–7434.

(12) Holt, D. A.; Luengo, J. J. I.; Yamashita, D. S.; Oh, H. J.; Konialian, A. L.; Yen, H. K.; Rozamus, L. W.; Brandt, M.; Bossard, M. J.; Levy, M. A.; Eggleston, D. S.; Liang, J.; Schultz, L. W.; Stout, T. J.; Clardyt, J. *J. Am. Chem. Soc.* **1993**, *115*, 9925–9938.

(13) Babine, R. E.; Bleckman, T. M.; Kissinger, C. R.; Showalter, R.; Pelletier, L. A.; Lewis, C.; Tucker, K.; Moomaw, E.; Parge, H. E.; Villafranca, J. E. *Bioorg. Med. Chem. Lett.* **1995**, *5*, 1719–1724.

(14) Chakraborty, T.; Weber, H. P.; Nicoloau, K. C. *Chem. Biol.* **1995**, *2*, 157–161.

(15) Hamilton, G.; Steiner, J. P. *Curr. Pharm. Des.* **1997**, *3*, 405–428.

(16) Dubowchik, G. M.; Vrudhula, V. M.; Dasgupta, B.; Ditta, J.; Chen, T.; Sheriff, S.; Sipman, K.; Witmer, M.; Tredup, J.; Vyas, D. M.; Verdoorn, T. A.; Bollini, S.; Vinitsky, A. *Org. Lett.* **2001**, *3*, 3987–3990.

(17) Wilkinson, D.; et al. *Bioorg. Med. Chem.* **2003**, *11*, 4815–4825.

(18) Holt, D. A.; Konialian-Beck, A. L.; Oh, H. J.; Yen, H. K.; Rozamus, L. W.; Krog, A. J.; Erhard, K. F.; Ortiz, E.; Levy, M. A.; Brandt, M.; Bossard, M. J.; Luengo, J. I. *Bioorg. Med. Chem. Lett.* **1994**, *4*, 315–320.

(19) Lamb, M. L.; W, L. J. *J. Med. Chem.* **1998**, *41*, 3928–3939.

(20) Wang, J.; Deng, Y.; Roux, B. *Biophys. J.* **2006**, *91*, 2798–2814.

(21) Lamb, M. L.; J. W., L.; Tirado-Rives, J. *Bioorg. Med. Chem.* **1999**, *7*, 851.

(22) Xu, Y.; Wang, R. *Proteins* **2006**, *64*, 1058–1068.

(23) Watanabe, H.; Tanaka, S.; Okimoto, N.; Hasegawa, A.; Taiji, M.; Tanida, Y.; Mitsui, T.; Katsuyama, M.; Fujitani, H. *Chem-Bio Inf. J.* **2010**, *10*, 32–45.

(24) Marinari, E.; Parisi, G. *Europhys. Lett.* **1992**, *19*, 451–458.

(25) Sugita, Y.; Okamoto, Y. *Chem. Phys. Lett.* **1999**, *314*, 141–151.

(26) Fukunishi, H.; Watanabe, O.; Takada, S. *J. Chem. Phys.* **2002**, *116*, 9058–9067.

(27) Marsili, S.; Signorini, G. F.; Chelli, R.; Marchi, M.; Procacci, P. *J. Comput. Chem.* **2010**, *31*, 1106–11161.

(28) Signorini, G. F.; Chelli, R.; Procacci, P.; Schettino, V. *J. Phys. Chem. B* **2004**, *108*, 12252–12257.

(29) Wiener, S. J.; Kollmann, P. A.; Nguyen, D. T.; Case, D. A. *J. Comput. Chem.* **1986**, *7*, 230.

(30) Duan, Y.; Wu, C.; Chowdhury, S.; Lee, M. C.; Xiong, G.; Zhang, W.; Yang, R.; Cieplak, P.; Luo, R.; Lee, T.; Caldwell, J.; Wang, J.; Kollman, P. *J. Comput. Chem.* **2003**, *24*, 1999–2012.

(31) Procacci, P.; Paci, E.; Darden, T.; Marchi, M. *J. Comput. Chem.* **1997**, *18*, 1848–1862.

(32) Stephens, P. J.; Devlin, F. J.; Chablowski, C. F.; Frisch, M. *J. Phys. Chem.* **1994**, *98*, 11623–11627.

(33) Singh, U. C.; Kollman, P. A. *J. Comput. Chem.* **1984**, *5*, 129–145.

(34) Liu, P.; Kim., B.; Friesner, R. A.; Berne, B. J. *Proc. Natl. Acad. Sci. U.S.A.* **2005**, *102*, 13749–13754.

(35) Jorgensen, W. L.; Chandrasekhar, J.; Madura, J.; Impey, R.; Klein, M. *J. Chem. Phys.* **1983**, *79*, 926–935.

(36) Nose, S. *J. Chem. Phys.* **1984**, *81*, 511–519.

(37) Marchi, M.; Procacci, P. *J. Chem. Phys.* **1998**, *109*, 5194–5202.
(38) Essmann, U.; Perera, L.; Berkowitz, M. L.; Darden, T.; Lee, H.; Pedersen, L. G. *J. Chem. Phys.* **1995**, *101*, 8577–8593.
(39) Tuckerman, M.; Berne, B. J.; Martyna, G. *J. Chem. Phys.* **1992**, *97*, 1990–2001.
(40) Ferrenberg, A.; Swendsen, R. H. *Phys. Rev. Lett.* **1989**, *63*, 1195.
(41) Jakalian, A.; Jack, D. B.; Bayly, C. I. *J. Comput. Chem.* **2002**, *23*, 1623–1641.
(42) Entrena, A.; Campos, J.; Gomez, J. A.; Gallo, M. A.; Espinosa, A. *J. Org. Chem.* **1997**, *62*, 337–349.
(43) Ponnuswamy, M. N.; Gromiha, M. M.; Sony, S. M. M.; Saraboji, K. *Topics in Heterocyclic Chemistry*; Springer-Verlag Publishers: Heidelberg, Germany, 2006.
(44) Shirts, M. R.; Chodera, J. D. *J. Chem. Phys.* **2008**, *129*, 124105.
(45) Bonomi, M.; Branduardi, D.; Bussi, G.; Camilloni, C.; Provasi, D.; Raiteri, P.; Donadio, D.; Marinelli, F.; Pietrucci, F.; Brogli, R. A.; Parrinello, M. *Comput. Phys. Commun.* **2009**, *180*, 1961–972.
(46) Silla, E.; Tunon, I.; Pascual-Ahuir, J. L. *J. Comput. Chem.* **1991**, *12*, 1077–1088.
(47) Deng, Y.; Roux, B. *J. Chem. Theor. Comput* **2006**, *2*, 1255–1273.
(48) Stillinger, F. H.; Weber, T. A. *Phys. Rev. A* **1982**, *25*, 978−989.